

A CENSUS OF GAS OUTFLOWS IN TYPE 2 ACTIVE GALACTIC NUCLEI

HYUN-JIN BAE¹ AND JONG-HAK WOO^{2,3,4}

¹Department of Astronomy and Center for Galaxy Evolution Research, Yonsei University, Seoul 120-749, Republic of Korea; hjb@galaxy.yonsei.ac.kr and

²Astronomy Program, Department of Physics and Astronomy, Seoul National University, Seoul 151-742, Republic of Korea; woo@astro.snu.ac.kr

accepted to ApJ

ABSTRACT

We perform a census of ionized gas outflows using a sample of $\sim 23,000$ type 2 active galactic nuclei (AGNs) out to $z \sim 0.1$. By measuring the velocity offset of narrow emission lines, i.e., [O III] $\lambda 5007$ and $H\alpha$, with respect to the systemic velocity measured from the stellar absorption lines, we find that 47% of AGNs display an [O III] line-of-sight velocity offset $\geq 20 \text{ km s}^{-1}$. The fraction of the [O III] velocity offset in type 2 AGNs is comparable to that in type 1 AGNs after considering the projection effect. AGNs with a large [O III] velocity offset preferentially have a high Eddington ratio, implying that the detected velocity offsets are related to black hole activity. The distribution of the host galaxy inclination is clearly different between the AGNs with blueshifted [O III] and the AGNs with redshifted [O III], supporting the combined model of the biconical outflow and dust obscuration. In addition, for $\sim 3\%$ of AGNs, [O III] and $H\alpha$ show comparable large velocity offsets, indicating a more complex gas kinematics than decelerating outflows in a stratified narrow-line region.

Subject headings: galaxies: active — galaxies: kinematics and dynamics

1. INTRODUCTION

Supermassive black holes (SMBHs) and their host galaxies show relatively tight scaling relationships in the local Universe (e.g., Ferrarese & Merritt 2000; Gebhardt et al. 2000; Gültekin et al. 2009; McConnell & Ma 2013; Kormendy & Ho 2013; Woo et al. 2013), implying the coevolution of black holes and their host galaxies. While theoretical studies suggested that mechanical and/or radiative feedback from active galactic nuclei (AGNs) regulate the growth of their host galaxies (e.g., Croton et al. 2006; Ciotti et al. 2009; Puchwein & Springel 2013; Shankar et al. 2013; Dubois et al. 2013), gas outflows detected in quasars may indicate the AGN feedback in action (e.g., Greene et al. 2012). Since AGN-driven outflows can significantly influence the surrounding interstellar medium (ISM) and star formation, observational constraints of the outflows are of importance in understanding SMBH-galaxy coevolution as well as the AGN feedback.

One of the tracers of gas outflows in AGNs is the line-of-sight velocity offset (v_{off}) of narrow emission lines with respect to the systemic velocity of host galaxies (e.g., Boroson 2005; Barbosa et al. 2009; Müller-Sánchez et al. 2011). In particular, the velocity offset of the strong [O III] $\lambda 5007$ narrow emission-line has long been of interest for probing AGN-driven outflows (e.g., Crenshaw & Kraemer 2000; Zamanov et al. 2002; Boroson 2005; Komossa et al. 2008; Crenshaw et al. 2010; Zhang et al. 2011). A number of high spatial resolution studies on nearby Seyfert galaxies reported decelerating radial gas motion in the narrow-line region (NLR), which were generally interpreted as AGN-driven biconical outflows (e.g., Crenshaw & Kraemer 2000; Crenshaw et al. 2000; Ruiz et al. 2001, 2005; Das et al. 2005; Fischer et al.

2010, 2013). Using Seyfert 1 galaxies and quasars, several groups have performed statistical investigations on the velocity offset of [O III] based on single-aperture spectra (e.g., Boroson 2005; Komossa et al. 2008; Crenshaw et al. 2010; Zhang et al. 2011). For example, Boroson (2005) studied the [O III] velocity offset of ~ 400 quasars selected from Sloan Digital Sky Survey (SDSS), suggesting that the radial velocity of [O III]-emitting gas is governed by both black hole mass and the Eddington ratio. Komossa et al. (2008) showed that the [O III] lines of narrow-line Seyfert 1 galaxies are blueshifted with respect to the low-ionization lines, which is consistent with the decelerating outflows in the stratified NLR (e.g., Crenshaw & Kraemer 2000; Ruiz et al. 2005). In this scenario inner high-ionization lines, e.g., [O III], show large radial velocity while outer low-ionization lines show no or smaller radial velocity (Komossa et al. 2008). For type 1 AGNs, however, it is not clear whether low-ionization lines are also shifted with respect to the systemic velocity, since the systemic velocity is not generally measured, for example, from stellar absorption lines.

For type 2 AGN, in contrast, the velocity offsets of both high- and low-ionization lines can be simultaneously measured with respect to the systemic velocity of their host galaxies using the stellar absorption lines. Nevertheless, AGN-driven outflows based on the velocity offset measurements have not been extensively studied for type 2 AGNs while there are several studies on the [O III] velocity offset with various limitations: some studies focused on a small sample (e.g., Comerford et al. 2009; Crenshaw et al. 2010), or individual objects (e.g., Crenshaw & Kraemer 2000; Sugai et al. 2005; Bae et al. 2012), and other studies used low-ionization lines to infer the systemic velocity (e.g., Wang et al. 2011). Interestingly, the results from these previous studies indicate the diverse origins of the [O III] velocity offsets. For a sample of 30 Seyfert 2 galaxies in DEEP2 survey, Comerford et al.

³ TJ Park Science Fellow

⁴ Author to whom any correspondence should be addressed

(2009) reported similar velocity offsets between the [O III] and the H β lines with respect to the stellar absorption lines, claiming that the velocity offsets are due to an inspiralling SMBH in merger remnants. Using a sample of 40 local Seyfert 2 galaxies, in contrast, Crenshaw et al. (2010) reported that the velocity offset of [O III] with respect to stellar lines is due to a combination of biconical outflows and dust extinction. Meanwhile, Wang et al. (2011) based on a large sample of $\sim 3,000$ SDSS type 2 AGNs argued that the velocity offset is not correlated with the Eddington ratio, which is in contrast to the results of the previous studies on type 1 AGNs (e.g., Boroson 2005; Komossa et al. 2008).

To investigate the statistical properties of gas outflows in type 2 AGNs, we perform a census of AGN-driven outflows by uniformly measuring the velocity offsets of narrow emission lines, i.e., [O III] and H α , with respect to the stellar absorption lines, using a large sample of type 2 AGNs selected from SDSS Data Release 7 (DR 7, Abazajian et al. 2009). The paper is constructed as follows. In Section 2, we describe our sample selection and analysis methods. Section 3 presents the main results on the velocity offsets. In Section 4, we compare our results with those of previous studies, and discuss the origin of the detected velocity offsets. Section 5 summarizes our findings. In the paper we adopt Λ CDM cosmological parameters, i.e., $H_o = 70 \text{ km s}^{-1} \text{ Mpc}^{-1}$, $\Omega_\Lambda = 0.73$, and $\Omega_m = 0.27$.

2. SAMPLE SELECTION & ANALYSIS

2.1. Sample selection

We utilized the SDSS DR 7 by matching the KIAS value-added galaxy catalog (Choi et al. 2010) and the MPA-JHU value-added catalog⁴ for the spectroscopic information. We selected galaxies at redshift range $0.02 < z < 0.1$ with signal-to-noise ratio (S/N) ≥ 10 for the continuum, and S/N ≥ 3 for the four emission lines, H β , [O III] $\lambda 5007$, H α , and [N II] $\lambda 6584$. Then the flux ratios of these four emission lines were used to classify AGNs (Baldwin et al. 1981). By adopting the demarcation line for AGNs and star-forming galaxies suggested by Kauffmann et al. (2003), we selected 60,018 type 2 AGN-host galaxies from the SDSS DR 7 catalog. As a comparison sample, we also selected $\sim 1,600$ star-forming galaxies with an additional constraint, $\log([\text{N II}]/\text{H}\alpha) < 0.7$, which was implemented to avoid a possible contamination of weak AGNs.

To ensure robust results on the AGN outflow statistics, we further restricted the sample by selecting AGNs that have reasonably small measurement uncertainty of the velocity offset. In general the radial velocity errors depend on the amplitude (peak)-to-noise ratio (A/N) of the targeted emission lines (Sarzi et al. 2006). Using the amplitude of the emission lines and the noise of the starlight-subtracted continuum at the 5030Å to 5130Å range, we calculated the A/N ratio for the [O III] and H α . Then we selected 24,356 AGNs with the A/N ratio ≥ 5 for both [O III] and H α , which is $\sim 41\%$ of the type 2 AGNs initially selected from the SDSS DR 7. In other words, we removed AGNs with weak emission lines, for which the measurement of the emission line velocity

offsets would not be reliable.

2.2. Velocity and Velocity Dispersion Measurements

We measured the velocity offset of the emission lines from the starlight-subtracted spectrum. To subtract the stellar absorption lines, we built a best-fit stellar template with the penalized pixel-fitting code (pPXF, Cappellari & Emsellem 2004), using 47 MILES simple stellar population models with solar metallicity and age spanning from 60 Myrs to 12.6 Gyrs (Sánchez-Blázquez et al. 2006). In this procedure we measured the velocity of the luminosity-weighted stellar component of the host galaxy (redshift), and adopted it as the systemic velocity. After constructing 100 mock galaxy spectra by randomizing the noise, we fit the stellar absorption lines for each spectrum to estimate the uncertainty. By adopting the $1\text{-}\sigma$ dispersion of measurements as the measurement error, we obtained the mean error of the systemic velocity as $\sim 9 \pm 5 \text{ km s}^{-1}$.

From the starlight-subtracted spectrum, we fit the narrow-emission lines, H α , H β , [N II]-doublet, [O I] $\lambda 6300$, and [O III] $\lambda 5007$, by utilizing MPFIT code (Markwardt 2009) with a single-Gaussian function. By performing visual inspection of the line fitting results, we removed any contamination from double-peaked line AGNs ($\sim 3.5\%$), type 1 AGNs with a broad H α line ($\sim 2.0\%$), or low-quality spectra/fitting ($\sim 0.5\%$), finalizing 22,906 AGNs as the final AGN sample. We find that $\sim 11\%$ AGNs in the final sample show the presence of a broad wing in the [O III] emission line profile. To improve the fitting results, we fit [O III] with a double-Gaussian function for these AGNs, and adopted the peak wavelength of the total profile as the representative center of the [O III] line. Finally, we calculated the velocity offset of each emission line by measuring the shift of the line peak with respect to the systemic velocity.

In addition to the velocity offset, we measured the line dispersion by calculating the second moment of the continuum-subtracted emission line profile:

$$\sigma_{line}^2(\lambda) = \frac{\int \lambda^2 f(\lambda) d\lambda}{\int f(\lambda) d\lambda} - \lambda_0^2 \quad (1)$$

where $f(\lambda)$ is the flux at each wavelength, and λ_0 is the first moment of the line. The measured line dispersions were corrected for the wavelength-dependent instrumental resolution of the SDSS spectroscopy, then converted to velocity.

To obtain the measurement error of the velocity and the line dispersion for each object, we constructed 100 mock spectra by randomizing the noise. By fitting the emission lines in each mock spectrum, we obtained the $1\text{-}\sigma$ dispersion of the measurements as the measurement error. For the AGN sample, the mean measurement error of the velocity is $\sim 16 \pm 10 \text{ km s}^{-1}$ and $\sim 7 \pm 7 \text{ km s}^{-1}$, respectively for [O III] and H α . In the case of the line dispersion, the mean measurement error is $\sim 23 \pm 35 \text{ km s}^{-1}$ and $\sim 10 \pm 10 \text{ km s}^{-1}$, respectively for [O III] and H α . By adding the errors of the emission line velocity and the systemic velocity in quadrature, we determined the total error of the velocity offset as $\sim 19 \pm 10 \text{ km s}^{-1}$ and $\sim 12 \pm 7 \text{ km s}^{-1}$, respectively for the [O III] and H α lines.

By performing the same error analysis for the star-forming galaxy sample, we obtained the systematic ve-

⁴ <http://www.mpa-garching.mpg.de/SDSS/>

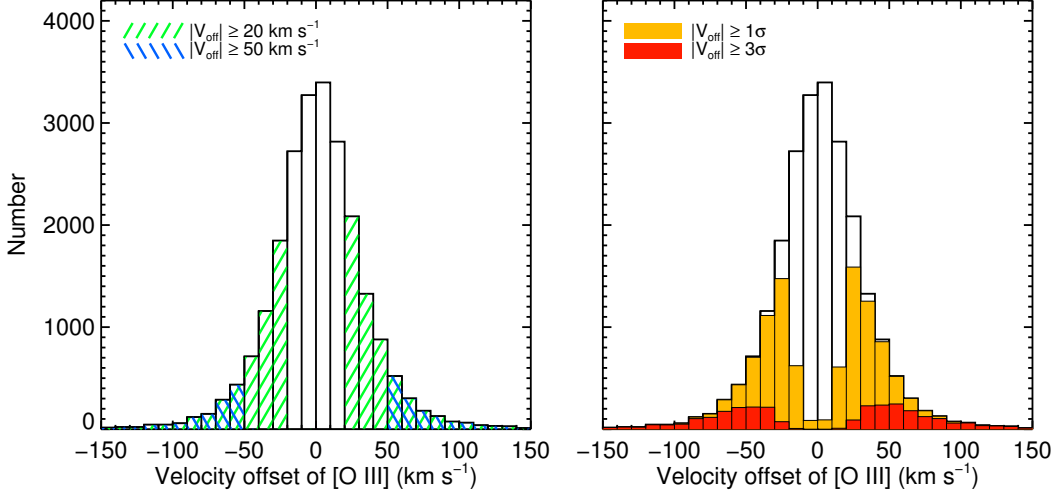


FIG. 1.— Distributions of the [O III] velocity offsets with respect to the systemic velocity for $\sim 23,000$ SDSS type 2 AGNs. The green- and blue-colored areas include AGNs with the velocity offset $\geq 20 \text{ km s}^{-1}$ and 50 km s^{-1} , respectively (left panel) while the orange- and red-colored areas include AGNs with the velocity offset larger than the measurement error (1σ and 3σ , respectively; right panel).

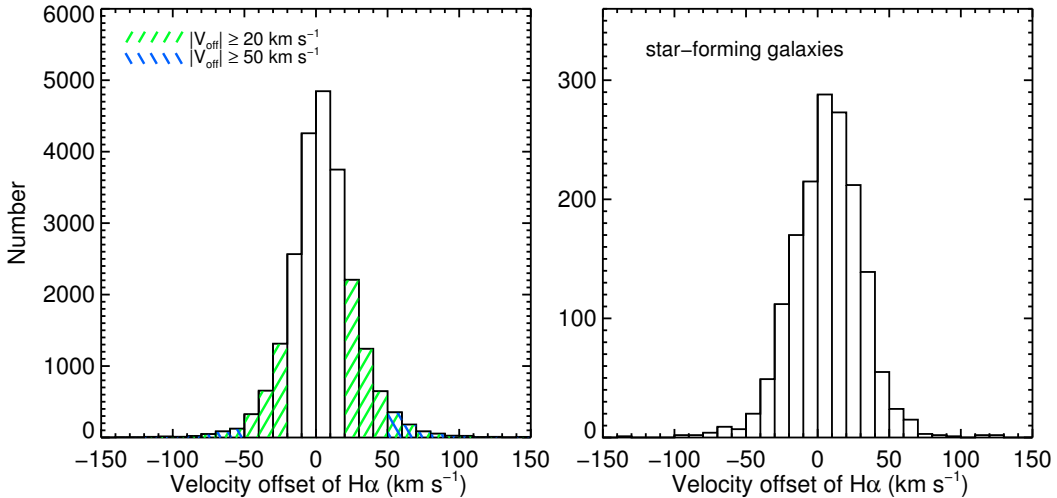


FIG. 2.— Distributions of the H α velocity offsets with respect to the systemic velocity for the AGN sample (left panel) and the star-forming galaxies (right panel). The green- and blue-colored areas include AGNs with the velocity offset $\geq 20 \text{ km s}^{-1}$ and 50 km s^{-1} , respectively.

locity error as $\sim 17 \pm 8 \text{ km s}^{-1}$, which is larger than the case of the AGN sample due to the higher uncertainty of the stellar population modeling. In the case of emission lines, we estimated the velocity error $\sim 4 \pm 3 \text{ km s}^{-1}$ and $\sim 1 \pm 1 \text{ km s}^{-1}$, respectively for [O III] and H α , and the line dispersion error $\sim 22 \pm 16 \text{ km s}^{-1}$ and $\sim 9 \pm 10 \text{ km s}^{-1}$, respectively for [O III] and H α .

3. RESULTS

3.1. Velocity offset of the narrow emission-lines

In Figure 1 (left), we present the distribution of the line-of-sight velocity offsets of [O III] with respect to the systemic velocity. The distribution shows a peak near 0 km s^{-1} with a dispersion $\sim 36 \text{ km s}^{-1}$. If we restrict the sample with the [O III] velocity offset $\geq 20 \text{ km s}^{-1}$ by considering the error of the velocity offset measurement (see Section 2.2), then 47% of AGNs show velocity offset.

If we further restrict the sample with the [O III] velocity offset $\geq 50 \text{ km s}^{-1}$, as often adopted for selecting outflows in the previous studies of type 1 AGNs (Boroson 2005; Komossa et al. 2008; Zhang et al. 2011), the fraction decreases to $\sim 12\%$. The lower fraction of the [O III] velocity offset in type 2 AGNs is expected from the unification model since the direction of the outflows is close to the plane of the sky. By considering the measurement uncertainty of the velocity offset for individual objects, we can also restrict the sample. In this case, the fraction of AGNs with the [O III] velocity offset with 3σ and 1σ detection is $\sim 12\%$ and $\sim 48\%$, respectively (Figure 1, right). We will further discuss the outflow statistics in Section 4.3.

While the [O III] emission line has been mainly used as an indicator of AGN outflows, the Balmer lines also show velocity offsets with respect to the systemic velocity. Fig-

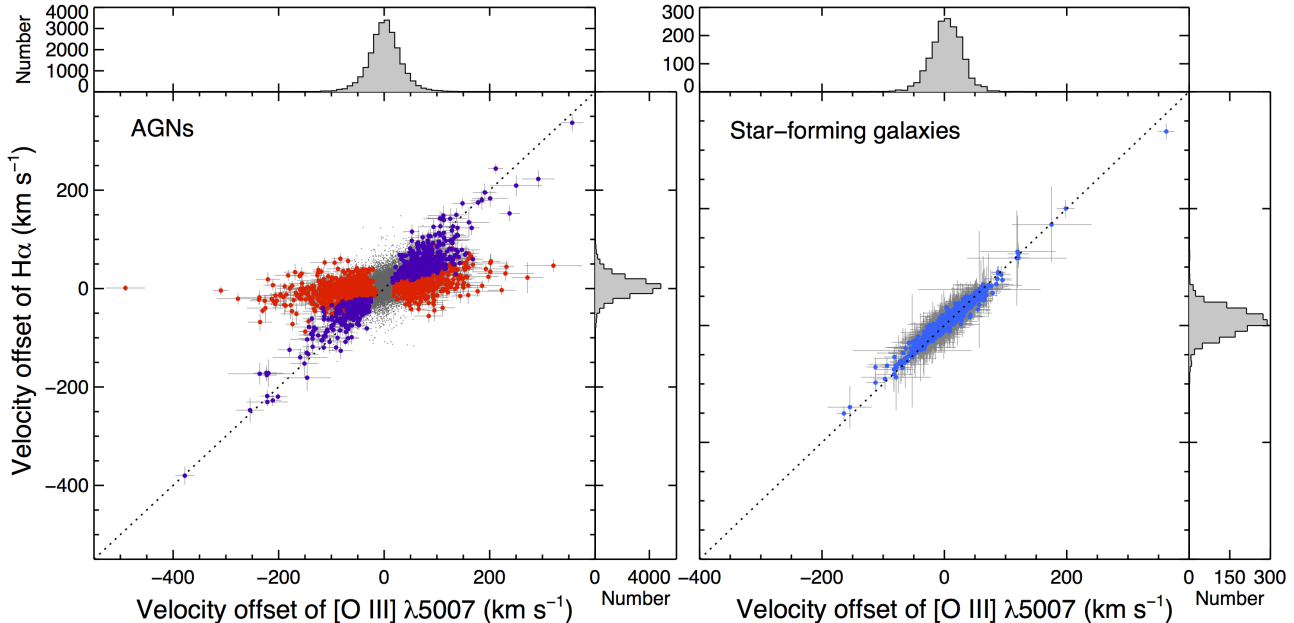


FIG. 3.— Comparison of the velocity offsets of [O III] and $H\alpha$ for AGNs (left) and star-forming galaxies (right). AGNs with the [O III] velocity offset detected with $3\text{-}\sigma$ limit are denoted with colored symbols while AGNs with no or weak ($< 3\text{-}\sigma$) [O III] velocity offset are represented by gray points. AGNs in Group A (red points) are defined i.e., the velocity difference between [O III] and $H\alpha$ is larger than $3\text{-}\sigma$ uncertainty, while AGNs in Group B (purple points) are defined with comparable velocities between [O III] and $H\alpha$ within $3\text{-}\sigma$ uncertainty. The one-to-one correspondence is denoted with the dotted lines.

ure 2 (left) presents the distribution of the line-of-sight velocity offsets of $H\alpha$, which shows a peak at $\sim 5 \text{ km s}^{-1}$ with a dispersion $\sim 25 \text{ km s}^{-1}$. The broader distribution of the [O III] velocity offsets than that of the $H\alpha$ velocity offsets may indicate that $H\alpha$ is less affected by AGN activity than the [O III] line. In the case of the $H\alpha$ offset fraction, $\sim 33\%$ ($\sim 5\%$) of AGNs show the velocity offset ≥ 20 (50) km s^{-1} , which is smaller than the case of [O III].

We note that, however, the $3''$ SDSS fiber size is larger ($1 - 6 \text{ kpc}$ depending on the redshift of object) than the typical size of the NLR ($< \sim 1 \text{ kpc}$). Hence, the spatially integrated spectra may also include star-forming regions outside of the active nuclei, although the flux-weighted line flux ratios indicate that the emission mainly originate from AGN. If this is the case, $H\alpha$ is more severely affected than [O III] by the contamination. For star-forming galaxies, the distribution of $H\alpha$ velocity offset shows a dispersion of $\sim 25 \text{ km s}^{-1}$, which is comparable to that of the AGN sample, supporting that the velocity of $H\alpha$ is possibly contaminated by the star-forming region in the gas disk.

3.2. Comparison of velocity offset

We compare the velocity offsets of [O III] and $H\alpha$ in Figure 3. For the majority of AGNs, the [O III] velocity offset is larger than that of $H\alpha$, while we find some fraction of AGNs with comparable velocity offset between [O III] and $H\alpha$. Note that the velocity difference between [O III] and $H\alpha$ has been used for identifying AGN outflows in the previous studies (e.g., Boroson 2005; Komossa et al. 2008; Crenshaw et al. 2010). We also find that $\sim 18\%$ of AGNs show effectively no velocity offset in both [O III] and $H\alpha$ ($< 1\text{-}\sigma$). For these AGNs, it is possible that the velocity offset is relatively weak or that

the gas motion effectively canceled out each other in the spatially integrated SDSS spectra.

To investigate the gas kinematics of [O III] in detail, we identify 2,855 AGNs with a robust [O III] velocity offset detection ($> 3\text{-}\sigma$) as shown with colored dots in Figure 3. As discussed in the previous section, the fraction of these AGNs is $\sim 12\%$ of the type 2 AGNs. For a large number of these AGNs, the velocity offset of $H\alpha$ is not detected ($< 3\text{-}\sigma$) or relatively weak compared to the [O III] velocity offset. Nevertheless, we find some fraction of AGNs, for which the $H\alpha$ velocity offset is detected ($> 3\text{-}\sigma$) and at the same time [O III] and $H\alpha$ show a comparable velocity offset (i.e., the velocity difference between [O III] and $H\alpha$ is less than $3\text{-}\sigma$ uncertainty) as shown with purple dots in Figure 3. Since the latter group of AGNs show distinct gas kinematics, we will compare them with the rest of AGNs. For this purpose, we call the AGNs with [O III] velocity offset larger than $H\alpha$ as Group A, while we call the AGNs with comparable velocities between [O III] and $H\alpha$ as Group B.

Group A is composed of 2,061 objects ($\sim 9\%$; red dots in Figure 3), showing relatively large [O III] velocity offsets compared to $H\alpha$ velocity offsets. Note that there are 495 AGNs in Group A, which show opposite signs between the [O III] and $H\alpha$ velocities. However, for most of these AGNs, the $H\alpha$ velocity offset is very weak ($\sim 10 \text{ km s}^{-1}$) and smaller than $3\text{-}\sigma$ uncertainty. Thus, it is not clear whether these AGN truly have opposite signs between [O III] and $H\alpha$ velocities. In contrast, 28 AGNs with a robust $H\alpha$ velocity offset detection ($> 3\text{-}\sigma$) show opposite signs between [O III] and $H\alpha$. It is possible that $H\alpha$ -emitting gas has dramatically different kinematics compared to [O III]-emitting gas in these AGNs. However, the velocity offset of these objects is on average very small (i.e., $H\alpha$ velocity offset = 36 km s^{-1}

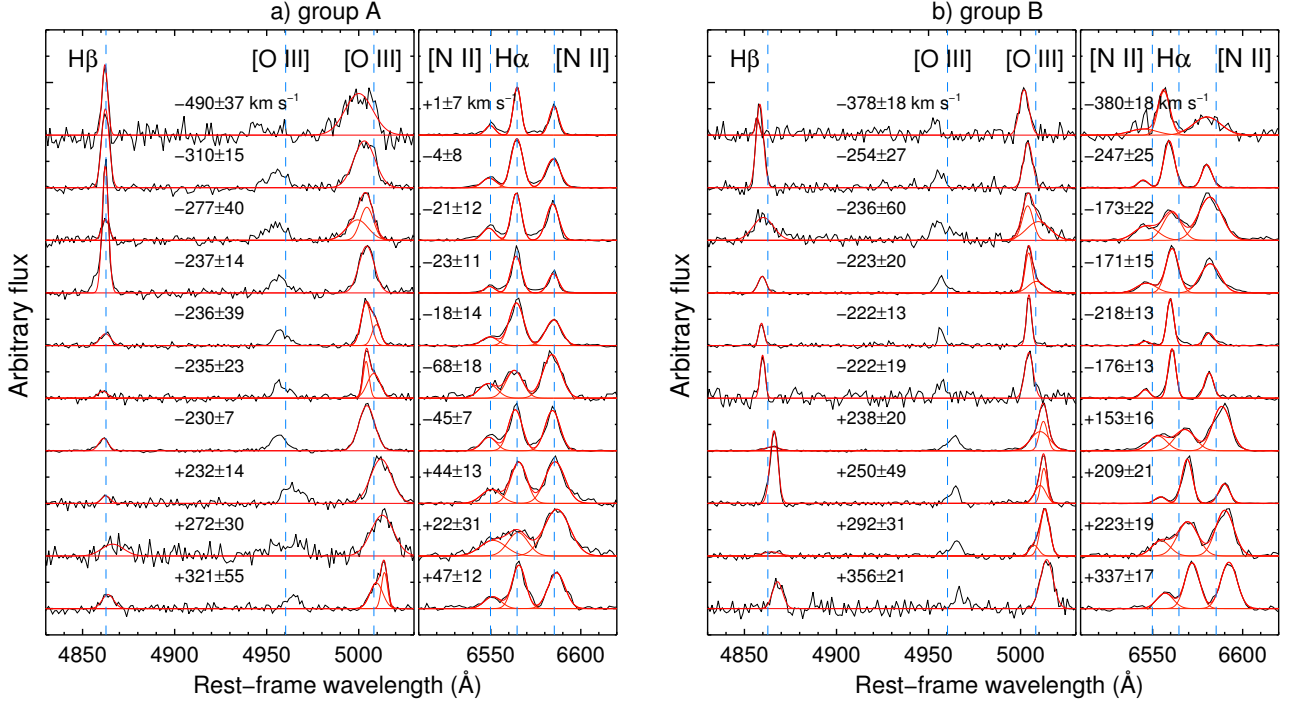


FIG. 4.— Examples of the starlight-subtracted spectra (black solid line) of 10 AGNs with the largest [O III] velocity offset in a) Group A, and b) group B. The best-fit models for the Balmer lines, the [N II]-doublet, and the [O III] line are overlaid (red and orange lines). The expected location of each emission line center based on the systemic velocity is indicated by blue dashed lines. The measured velocity offsets of [O III] and H α are indicated in each panel.

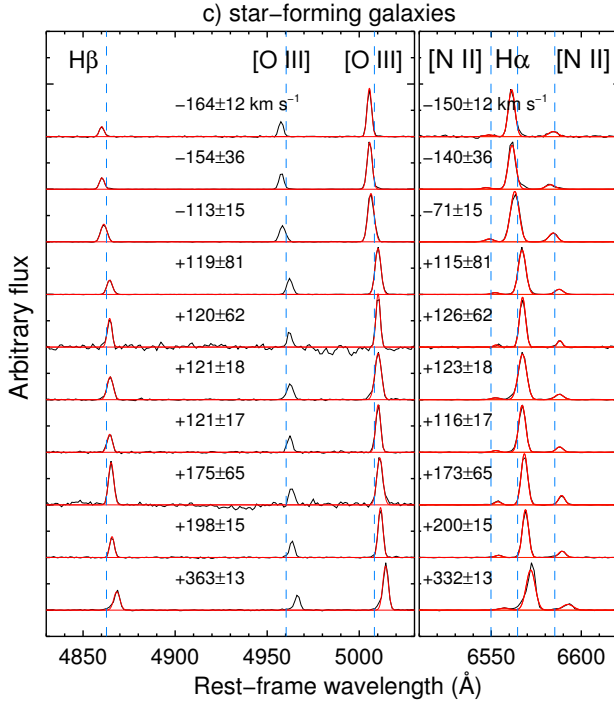


FIG. 4.— c) Examples of the starlight-subtracted spectra of 10 star-forming galaxies with the largest [O III] velocity offset.

with a standard deviation 10 km s^{-1} ; [O III] velocity offset = -68 km s^{-1} with a standard deviation 37 km s^{-1} ; note that all of them have redshifted H α and blueshifted [O III]. Although the origin of the opposite direction of the velocity offsets is not fully understood without spa-

tially resolved data, it is probably due to the more complex kinematics of the H α -emitting gas, which can be attributed by asymmetric distribution in a rotating disk, while the [O III]-emitting gas is mainly concentrated at the center. Since these AGNs are only 1% of Group A and the H α velocity offset is relatively small, we simply include them in Group A without further classification for the following analysis.

Group B consists of 794 AGNs ($\sim 3\%$; purple dots in Figure 3), showing that [O III] and H α have comparable velocities within the $3\text{-}\sigma$ uncertainty. If we change the definition of Group B with $2\text{-}\sigma$ uncertainty (i.e., the velocity difference between [O III] and H α $< 2\text{-}\sigma$), then the number of AGNs in Group B decreases to 727 objects while the number of AGNs in Group A increases to 2128 objects. However, the choice of the σ limit does not significantly change the results in the following analysis. There are AGNs with the velocity offset of H α larger than that of [O III], while the velocity difference between H α and [O III] is smaller than $3\text{-}\sigma$ for all AGNs in Group B. If we change the σ limit for the velocity difference between [O III] and H α , only 4 and 24 objects show larger H α velocity than [O III] velocity, respectively for $2\text{-}\sigma$ and $1\text{-}\sigma$ limit.

In Figure 4, we present the examples of the starlight-subtracted spectra, showing that the [O III] emission line is clearly shifted from the expected wavelength based on the systemic velocity, while the Balmer and the [N II] lines show no and similar offset, respectively for Group A and B.

In contrast, for star-forming galaxies [O III] and H α show comparable velocity offsets (Figure 4c) and we do not find any star-forming galaxies with significantly dif-

ferent velocities between [O III] and H α . This is dramatically different from the trend we described for the AGN sample. The distributions of [O III] and H α velocity offsets are similar with a $1\text{-}\sigma$ dispersion of $\sim 30 \text{ km s}^{-1}$. The galaxies with a large velocity offset ($\geq 30 \text{ km s}^{-1}$) present an asymmetric disk in the SDSS image, suggesting that the velocity offset detected in the spatially integrated spectra is presumably due to the asymmetric distribution of star-forming regions in the rotating disk. The fact that star-forming galaxies and Group B show similar H α velocity offsets with respect to [O III] may suggest that the H α velocity of Group B is also affected by star formation. However, star-forming galaxies and Group B do not necessarily have the same origin of the velocity offset since the emission line flux ratios are clearly different (see Section 2.1). Also, the dramatic difference in the distribution of the [O III] and H α line dispersions further supports that Group B may have a different origin (see Figure 5 and Section 3.3). Possible scenarios on the origin of the velocity offsets in Group B are further discussed in Section 4.2.

3.3. Comparison of line dispersion with velocity offset

We compare the line dispersions of [O III] and H α in Figure 5. In Group A, the [O III] line dispersions show a wide distribution (mean $\sim 161 \text{ km s}^{-1}$ and $1\text{-}\sigma$ dispersion $\sim 67 \text{ km s}^{-1}$) with a long tail toward the high line dispersion, while H α shows narrower distribution (mean $\sim 126 \text{ km s}^{-1}$ and $1\text{-}\sigma$ dispersion $\sim 38 \text{ km s}^{-1}$), suggesting the presence of high-velocity gas in the [O III]-emitting region. For individual AGNs, [O III] is on average $\sim 31\%$ broader than H α , indicating that the outflows with a wide opening angle contributes to the line-of-sight velocity dispersion of [O III] while the H α line is less affected. The large [O III] line dispersions are mostly related to the presence of a broad wing in the line profile (open circles). In the case of Group B, the line dispersions of [O III] and H α are similar to each other except for a small number of outliers.

In contrast, the star-forming galaxies show much narrower emission lines than AGNs, and comparable line dispersions between [O III] and H α (Figure 5, right panel), as expected from the lack of asymmetric broad wing features (see Figure 4c). Although most of the resolution-corrected line dispersions are below the SDSS instrumental resolution, it is clear that [O III] and H α in star-forming galaxies have comparable random velocities while [O III] in AGNs has a systematically larger random velocity than H α .

In Figure 6, we compare the velocity offset with the line dispersion. In Group A, large [O III] velocity offsets are preferentially found among AGNs with large line dispersion, implying that the [O III] line widths are also increased due to the AGN-driven outflows, while such a trend is weaker in Group B.

The gravitational potential of the galaxy bulge is mainly responsible for the broadening of the [O III] emission line when the outflow is not dominant as shown by the previous works in comparing the [O III] line widths with stellar velocity dispersions (e.g., Nelson & Whittle 1995; Komossa & Xu 2007). When AGN outflow is strong, however, the emission lines can be additionally broadened due to the gas motion in biconical outflows

with a wide opening angle, as manifested by the presence of broad wings in the [O III] emission line profile.

We note that some AGNs in Group A show large [O III] line dispersions ($\geq 300 \text{ km s}^{-1}$), and relatively low velocity offsets ($< 100 \text{ km s}^{-1}$). Most of these objects have a broad wing in the [O III] line profile (open circles), indicating the presence of high velocity gas. It is possible that the outflow direction of these objects is almost perpendicular to the line-of-sight, resulting in a small projected velocity offset while the line width is additionally broadened due to the radial gas motion in a wide opening angle, which includes blueshifted and redshifted components to the line-of-sight.

The trend between velocity offset and line dispersion can be also related to the dust obscuration (Crenshaw et al. 2010). Dust-patches in the inner stellar disk may preferentially obscure one side of the biconical outflows, depending on the orientation angle between the stellar disk and the outflow direction, hence either blueshifted or redshifted velocity offset is detected in the luminosity-weighted integrated spectroscopic observations. If there is a biconical outflow and no internal dust extinction, one may find a larger line width than expected from the galaxy bulge potential, while no significant velocity offset is expected since the approaching and receding gas motions will cancel out each other.

3.4. Velocity offset vs. Eddington ratio

In this section we compare the [O III] velocity offset with the Eddington ratio. We calculate AGN bolometric luminosity using the equation suggested by Netzer (2009) for type 2 AGNs:

$$\log L_{\text{bol}} = 3.8 + 0.25 \log L([\text{O III}]\lambda 5007) + 0.75 \log L([\text{O I}]\lambda 6300), \quad (2)$$

where $L([\text{O III}]\lambda 5007)$ and $L([\text{O I}]\lambda 6300)$ are the extinction-corrected luminosities of [O III] and [O I], respectively. We correct for extinction using the extinction law suggested by Calzetti (1999), assuming the intrinsic Balmer decrement $\text{H}\alpha/\text{H}\beta = 2.86$ (Netzer 2009). For this calculation, $\sim 13\%$ of AGNs have been excluded due to the non-detection of [O I] emission. As a consistency check, we also calculate the bolometric luminosity using the equation $L_{\text{bol}} = 700 \times L([\text{O III}]\lambda 5007)$ (LaMassa et al. 2009), where the [O III] luminosity is also extinction-corrected. We use the stellar velocity dispersion (σ_*) available from MPA-JHU catalog to infer black hole mass (M_{BH}) by adopting the $M_{\text{BH}}\text{-}\sigma_*$ relation (Park et al. 2012; Woo et al. 2013).

We find that the Eddington ratio distributions are different between the two groups. In Group A, AGNs with large velocity offsets preferentially have a high Eddington ratio, while the trend is not found in Group B (see Figure 7). When we use the [O III] luminosity as a proxy for the AGN bolometric luminosity, we obtain qualitatively the same results.

To examine the trend in detail, we divide the sample into five bins with different Eddington ratio range (see Table 1). In Group A the fraction of the detected velocity offset largely increases from 1% to 17% as the Eddington ratio increases, while Group B does not show such a trend. Although the estimated Eddington ratios have large uncertainties, our results are consistent with that

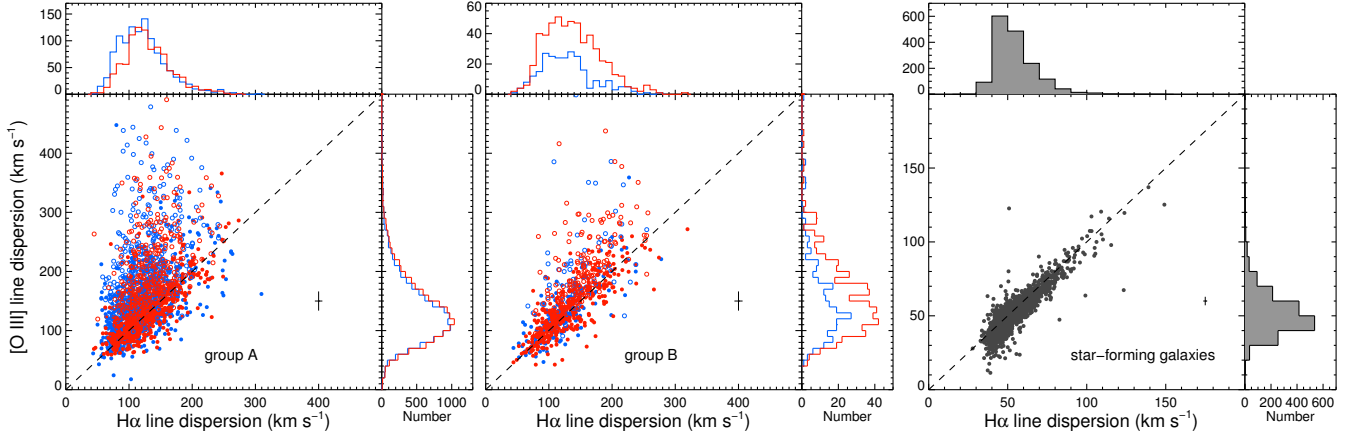


FIG. 5.— Comparison of the line dispersions between [O III] and H α for Group A (left), Group B (middle), and the star-forming galaxies (right). Blue and red dots represent AGNs with the blueshifted- and redshifted [O III], respectively while open (filled) circles indicate the presence (absence) of an asymmetric wing feature in the [O III] line profile. The mean errors of the line dispersion measurements are denoted at the bottom right. Note that the dispersion range for the star-forming galaxies is a factor of two smaller than that of AGNs.

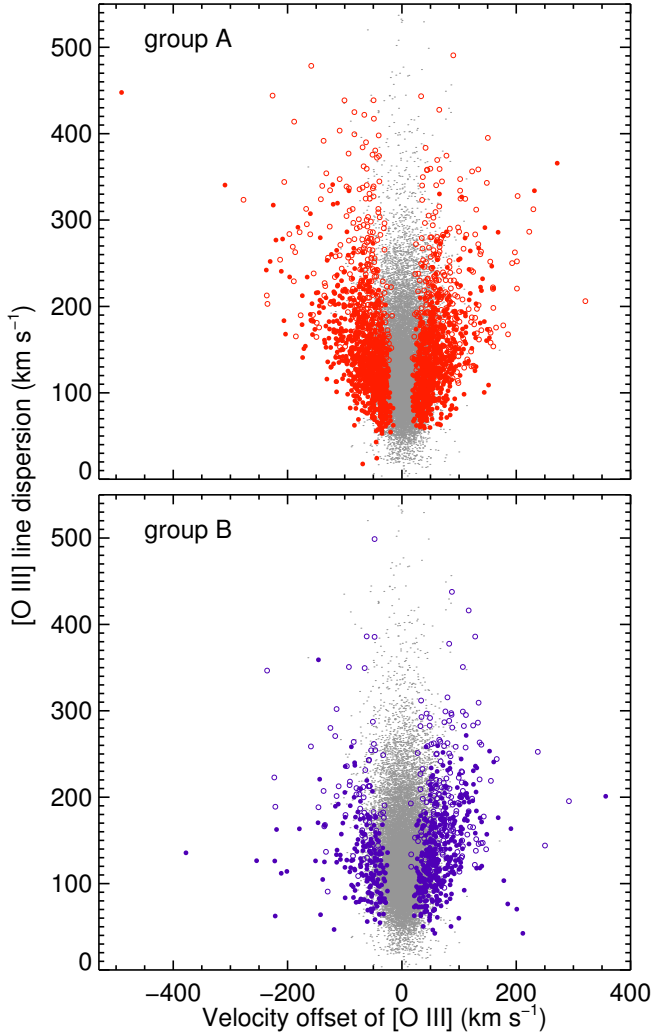


FIG. 6.— Comparison of the velocity offset and line dispersion of [O III] for Group A (top) and Group B (bottom). Symbols are the same as in Figure 3.

TABLE 1
NUMBER OF AGNs IN VARIOUS EDDINGTON RATIO RANGES

ER (1)	Total (2)	A+B (3)	Group A (4)	Group B (5)
> 1	1350	293 (22%)	236 (17%)	57 (4%)
$0.1 - 1$	7897	1391 (18%)	1068 (14%)	323 (4%)
$0.01 - 0.1$	7060	806 (11%)	518 (7%)	288 (4%)
$0.001 - 0.01$	2550	120 (5%)	68 (3%)	52 (2%)
< 0.001	1062	29 (3%)	13 (1%)	16 (2%)

NOTE. — (1) Range of the Eddington ratios; (2) Number of the total AGNs within the Eddington ratio range; (3) Number (fraction) of both group A and B within the Eddington ratio range (4) Number (fraction) of the group A within the Eddington ratio range; (5) Number (fraction) of the group B within the Eddington ratio range.

the detected velocity offsets are due to AGN activity.

While we find that AGNs with a large [O III] velocity offset preferentially have a high Eddington ratio, we also find AGNs with a high Eddington ratio, but with a small velocity offset. One of the possible explanations is that the low velocity offset is due to a projection effect when the outflow direction is close to the plane of the sky. Another possibility is that the blueshifted and redshifted components are canceled out in the spatially integrated SDSS spectra if the dust in the stellar disk does not strongly obscure one side of the biconical outflows.

3.5. Inclination of the host galaxies

The detected [O III] velocity offset can be explained with a combined model of biconical outflows and dust extinction in the host galaxy disk (Crenshaw et al. 2010). Since dust-patches in the disk can preferentially obscure one side of the biconical outflows, depending on the orientation angle between the direction of outflows and the disk plane, either blueshifted or redshifted [O III] will be detected in the spatially integrated spectra.

As a consistency check, we investigate the distribution

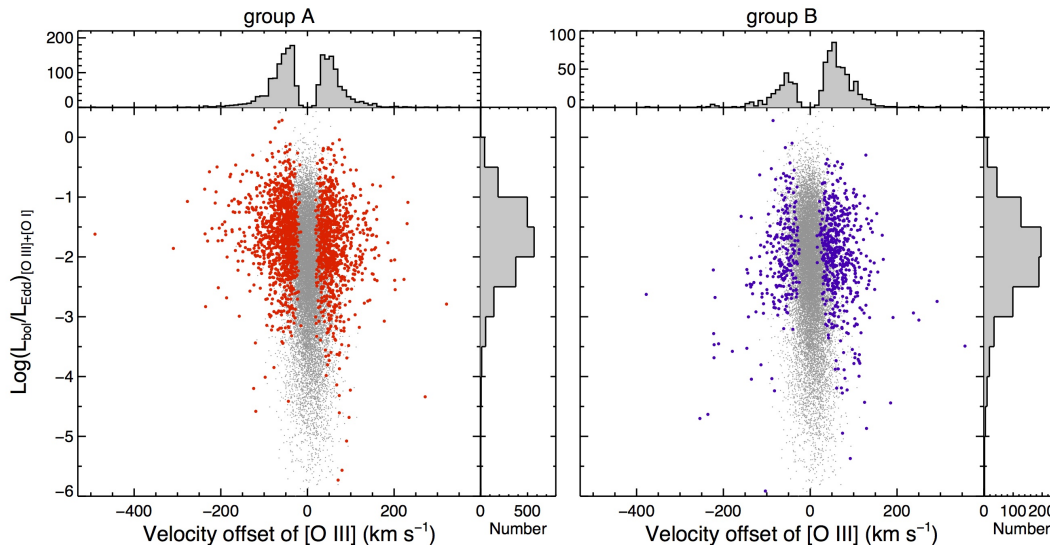


FIG. 7.— Comparison of the [O III] velocity offset with the Eddington ratio for Group A (left), and Group B (right panels). Symbols are the same as in Figure 3.

of the host galaxy inclination, respectively for the AGNs with blueshifted and redshifted [O III]. If the outflows are biconical, we expect that more AGNs with blueshifted [O III] will be detected in face-on late-type galaxies since the redshifted component can be obscured by the dust in the disk. First, we choose late-type galaxies ($\sim 40\%$) among the AGN sample, based on the visual morphology classification from Lintott et al. (2011). Second, we measure the seeing-corrected isophotal minor-to-major axis ratio b/a on the SDSS i -band image. For comparison, we also obtain the distribution of the axis ratio for all late-type AGN host galaxies in the SDSS DR 7.

By applying a Gaussian kernel, we present the normalized probability distributions in Figure 8. In Group A, the distribution is clearly different between the AGNs with redshifted [O III] and the AGNs with blueshifted [O III], particularly when b/a is larger than 0.5, indicating that face-on galaxies are more likely to host AGNs with blueshifted [O III]. While the distribution of the AGNs with blueshifted [O III] is similar to that of the general population of late-type AGN host galaxies, the relative lack of the AGNs with redshifted [O III] is consistent with the combined model of the bipolar outflow and dust obscuration. Since the angle between the disk plane and the outflow direction is random, galaxies with intermediate inclinations can obscure either blueshifted or redshifted [O III] with similar probability. As expected, no clear difference is found at intermediate b/a . In the case of Group B, on the contrary, AGN with blueshifted and redshifted [O III] show a lack of face-on host galaxies, compared to the general population of late-type AGN host galaxies. This may suggest that Group B galaxies are not representative of general AGN host galaxy population (see discussion in Section 4.2).

3.6. Radio properties

We investigate whether the [O III] velocity offsets are related to radio jets using the FIRST survey catalog (White et al. 1997). Similarly in both Group A and Group B, $\sim 25\%$ of AGNs have a radio counterpart. Among the detected sources, only $\sim 1\%$ of AGNs show

clear jet-like or elongated radio morphology, while the others look more or less compact (with a beam size $\sim 5''$). The radio detection rate increases with the increasing [O III] velocity offset. In Group A, the detection rate is 17%, 26%, and 40% respectively for AGNs with the [O III] velocity offset smaller than 50 km s^{-1} , between 50 and 100 km s^{-1} , and larger than 100 km s^{-1} . A similar trend is also found in Group B. The results imply that radio jets are related with the ionized gas outflows at least for the radio-detected AGNs.

4. DISCUSSION

4.1. Starburst-driven vs. AGN-driven Outflows

Although the photoionizing source of the narrow emission lines is likely to be AGNs for given the emission line flux ratios used for our sample selection, the nature of the velocity offsets manifested by these lines are not straightforward to interpret. For instance, since AGNs and nuclear star formation activities are often coupled (e.g., Nath & Silk 2009; Netzer 2009; Woo et al. 2012), the observed velocity offsets can be due to the outflows from the nuclear starburst.

One of the main differences between AGN- and starburst-driven outflows is the geometry of the outflows; while the AGN-driven outflows are randomly oriented with respect to the host galaxy, the direction of the starburst-driven outflows is in general perpendicular to the stellar disk (Veilleux et al. 2005, and references therein). Thus, if the detected velocity offsets are attributed to the starburst, the majority of spiral galaxies with intermediate to face-on inclinations (i.e., $b/a \geq 0.6$) are expected to show blueshifted [O III]. On the contrary, we find that $\sim 38\%$ and $\sim 68\%$ of the late-type galaxies with $b/a > 0.6$, respectively in Group A and Group B, show redshifted [O III], suggesting that the detected velocity offsets are not starburst-driven. Moreover, in the case of starburst-driven outflows, face-on galaxies should have larger line-of-sight velocities than edge-on galaxies since the outflow direction is closer to the line-of-sight. On the contrary, we find that the mean [O III] velocity is smaller by $\sim 10\%$ and $\sim 20\%$ in more inclined galaxies

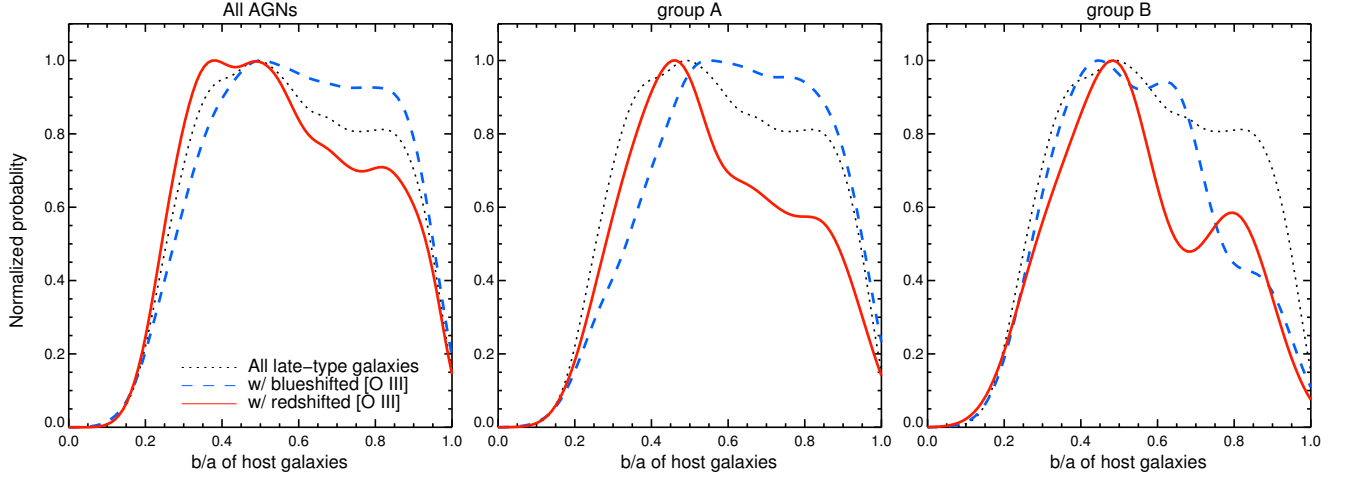


FIG. 8.— Normalized probability distributions of the axis ratio (b/a) respectively for AGNs with the blueshifted (blue dashed line) and redshifted $[\text{O III}]$ (red solid line). The distributions are shown for the total sample (left), Group A (middle), and Group B (right). The black dotted line represents all late-type AGN host galaxies from SDSS DR 7.

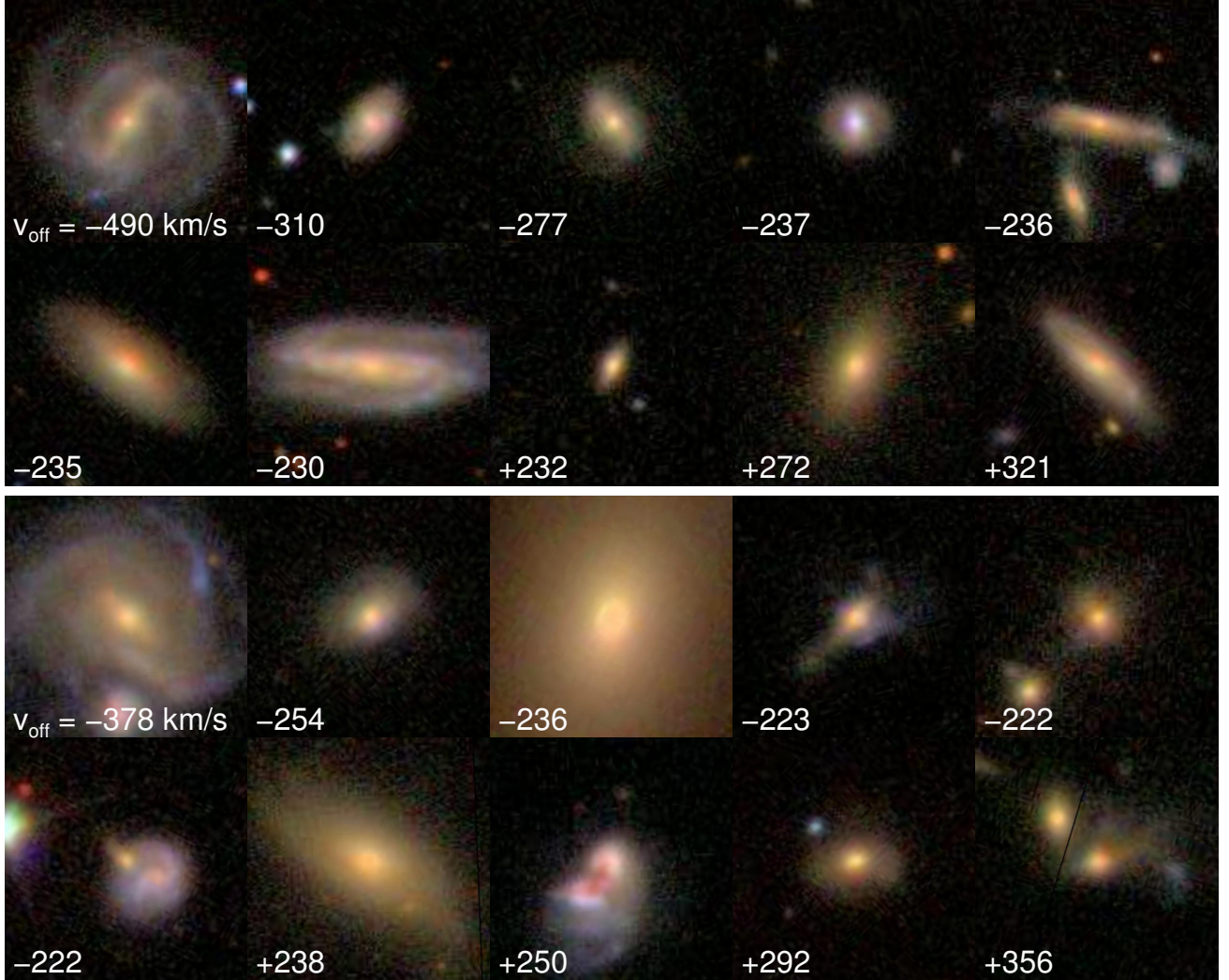


FIG. 9.— SDSS gri-composite images of the galaxies with the largest $[\text{O III}]$ velocity offset: 10 AGNs in Group A (top) and 10 AGNs in Group B (bottom). The $[\text{O III}]$ velocity offset is labeled in each $40'' \times 40''$ size panel.

($b/a \geq 0.6$) than in more face-on galaxies ($b/a < 0.6$), respectively for Group A and Group B. Thus, we conclude that the velocity offset of [O III] is not likely due to the nuclear starburst.

4.2. Nature of the velocity offset in the group B

As presented in Section 3.2, for a small fraction of AGNs, [O III] and H α show comparable velocity offsets with respect to the systemic velocity. The [O III] velocity offsets can be interpreted as AGN-driven, since the emission line flux ratios are consistent with the AGN photoionization. However, the origin of the comparable velocity offset of H α is unclear. One possibility is that the deceleration of the outflows is much weaker and/or gas outflows are significant in the outer NLR so that H α and other low-ionization lines have comparable velocity offsets as [O III]. While the deceleration is expected if the outflows interact with the surrounding ISM (De Young 2010), the deceleration may not be strong in certain physical conditions, such as with a lower ISM density, or with more energetic outflows.

We note that the host galaxies of Group B tend to have disturbed morphology and merging features, particularly for the AGNs with a large [O III] velocity offset; for example, $\sim 54\%$ of AGNs with the [O III] velocity offset ≥ 100 km s $^{-1}$, and all AGNs with the [O III] velocity offset ≥ 200 km s $^{-1}$ in Group B present signatures of on-going or recent merger (e.g., see Figure 9), indicating that these galaxies are going through a dramatic dynamical process, presumably accompanied by a strong starburst activity. In such a case, it is possible that the non-virialized stars and gas are kinematically decoupled, resulting in the velocity offset between stellar absorption lines and the gas emission lines.

Another possibility is that the velocity offset is caused by a binary black hole system, consisting of an inactive black hole and an active black hole, which is either inspiralling (Milosavljević & Merritt 2001) or recoiling (Campanelli et al. 2007), and displaced from the dynamical center of the host galaxy. In the latter case, however, theoretical studies showed that the black hole could not have a large enough radius to carry the NLR after the kick (Merritt et al. 2006). Instead, the inspiralling active black hole with an accompanied NLR may be a viable explanation for the velocity offset (e.g., Comerford et al. 2009; Comerford & Greene 2014). Recently, Comerford & Greene (2014) find ~ 400 AGNs in SDSS showing comparable velocity offsets between the forbidden lines and the Balmer lines, which are similar to the AGNs in Group B, claiming that the AGNs are candidates for kinematically offset SMBH.

Using the N-body simulations, Blecha et al. (2013) showed that during the galaxy-galaxy merging, spectroscopic observations may detect only one NLR with a significant (a few hundred km s $^{-1}$) velocity offset, depending on physical properties, i.e., the galaxy mass ratio, gas content, and the viewing angle. If the velocity offset detected in our analysis is due to the binary motions, the projected distance between the two black holes could be a few kpc (Comerford et al. 2009; Shen et al. 2011). Considering the $3''$ aperture size of the SDSS spectroscopy, which covers several kpc of the targets, it is possible that the displaced active black hole and its NLR are observed

through the SDSS fiber. In this scenario, it is difficult to detect two active black holes since only one black hole is active for the majority of the merging time. Instead, the presence of double stellar cores may provide circumstantial evidence (Shen et al. 2011). We investigated the morphology of the 142 AGNs with the largest (> 100 km s $^{-1}$) velocity offsets in Group B, using the SDSS gr-composite images. We find double stellar cores only in $\sim 5\%$ of the AGNs, suggesting that the displaced black hole scenario is not well supported for Group B.

4.3. AGN Outflow Statistics

In this study, we find that $\sim 47\%$ of $\sim 23,000$ type 2 AGNs have an [O III] velocity offset larger than 20 km s $^{-1}$ with respect to the systemic velocity. If we interpret the velocity offset as due to AGN outflows, the AGN outflow fraction based on the detected velocity offset is a lower limit because of a couple of limitations. First, we only count the outflows when the velocity offset is larger than 20 km s $^{-1}$ by accounting for the uncertainties of the velocity offset measurement. Second, the measured velocity offset is the line-of-sight velocity. Thus, if the outflow direction is very close to the plane of the sky, we do not detect the offset in the line-of-sight. Third, if the blueshifted and redshifted cones are symmetric and canceled out each other in the spatially integrated spectra, we do not detect the velocity offsets with respect to systemic velocity.

With these limitations, we compare the fraction of the AGN-driven outflows between type 1 and type 2 AGNs by combining the results from the literature. Various previous studies reported that $\sim 50\%$ of type 1 AGNs show outflows although the analysis methods were not uniform. For example, Boroson (2005) reported that approximately a half of ~ 400 SDSS QSOs has blueshifted [O III] while Komossa et al. (2008) presented that 51% (28 out of 55) of narrow-line Seyfert 1 galaxies have the [O III] velocity offset larger than 50 km s $^{-1}$. A more recent study by Zhang et al. (2011) reported that 69% of ~ 400 Seyfert 1 galaxies show the [O III] velocity offset larger than 50 km s $^{-1}$. Using a much smaller sample of 20 Seyfert 1 galaxies based on the observations of Nelson & Whittle (1995), Crenshaw et al. (2010) reported that 50% of Seyfert 1 galaxies have the [O III] velocity offset larger than 50 km s $^{-1}$.

In the case of type 2 AGNs, Crenshaw et al. (2010) presented that 17 out of 45 (38%) Seyfert 2 galaxies have the velocity offset larger than 50 km s $^{-1}$ while Wang et al. (2011) showed that $\sim 25\%$ of $\sim 3,000$ type 2 AGNs from SDSS have the [O III] velocity offset above 50 km s $^{-1}$. Note that the velocity offset in the study of Wang et al. (2011) was measured with respect to the low-ionization lines. If we measure the [O III] velocity offset with respect to the H α lines using our AGN sample, $\sim 9\%$ of AGNs show the velocity offset ≥ 50 km s $^{-1}$ (see Figure 10), which is lower than that of Wang et al. (2011). One of the possible explanations for the difference is that their sample is biased toward the AGNs with high [O III] fluxes due to their selection with $S/N \geq 30$ for [O III], while our sample includes AGNs with much weaker [O III].

Compared to type 1 AGNs, the outflow fraction of type 2 AGNs is generally lower for a fixed velocity offset limit (i.e., 50 km s $^{-1}$). This can be explained as the orienta-

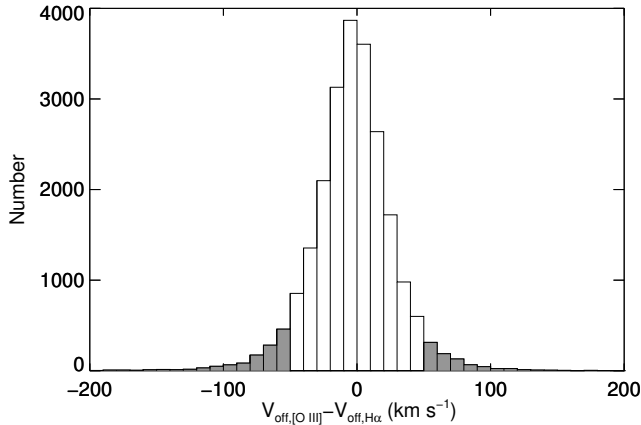


FIG. 10.— Distribution of the velocity difference between [O III] and H α . The shaded region indicates the AGNs with the velocity offset $\geq 50 \text{ km s}^{-1}$.

tion effect (Antonucci & Miller 1985) since the projected outflow velocity to the line-of-sight is on average lower in type 2 AGNs than in type 1 AGNs. The direct comparison of the outflow fraction between type 1 and type 2 AGNs is beyond the scope of this study since the consistent measurements of the [O III] velocity offsets with respect to the systemic velocity (e.g., based on stellar absorption lines) are also required for type 1 AGNs.

5. SUMMARY & CONCLUSION

Using a large sample of $\sim 23,000$ type 2 AGNs, we perform a census of the ionized gas outflows by measuring the velocity offset of narrow emission lines with respect to the systemic velocity measured from the stellar absorption lines. We summarize the main results as follows.

- We find that $\sim 47\%$ of type 2 AGNs display an [O III] line-of-sight velocity offset larger than 20 km s^{-1} with respect to the systemic velocity.
- AGNs with larger [O III] velocity offsets, in particular with no or weak H α velocity offsets, tend to have higher Eddington ratios, implying that the [O III] velocity offset is related to on-going black hole activity. The presence of high Eddington ratio AGNs with relatively small [O III] velocity offsets implies a projection effect,

which can significantly decreases the line-of-sight velocity if the outflow direction is close to the plane of the sky.

- Face-on galaxies preferentially host the AGNs with blueshifted [O III] (rather than the AGNs with redshifted [O III]), presumably due to the dust obscuration in the host galaxy disk. The difference of the galaxy inclinations between the AGNs with blueshifted and the AGNs with redshifted [O III] lines, supports the combined model of the biconical outflow and dust obscuration.

- The outflow fraction in type 2 AGNs is a lower limit, considering the detection limit of the velocity offset and the projection effect. For a fixed limit of the velocity offset (i.e., $> 50 \text{ km s}^{-1}$), type 2 AGNs have a lower outflow fraction than type 1 AGNs due to the projection.

- We find that for $\sim 3\%$ of AGNs, H α and [O III] show comparable velocity offsets, suggesting non-decelerating outflows and/or more complex gas kinematics in the NLR geometry, e.g., off-centered AGNs.

Based on these results, we conclude that the ionized gas outflows are common in AGNs. The sample of the AGN-driven outflows with a large [O III] velocity is one of the best suites for studying AGN feedback and the role of AGNs in the coevolution of SMBHs and their host galaxies. Follow-up observations with high spatial resolution will provide detailed information on the kinematics and geometry of the NLR as well as the properties of ISM and the stellar populations in the host galaxies.

We thank the anonymous referee for valuable comments, which improved the presentation and clarity of the paper. The work of HJB was supported by NRF (National Research Foundation of Korea) Grant funded by the Korean Government (NRF-2010-Fostering Core Leaders of the Future Basic Science Program). JHW acknowledges the support by the National Research Foundation of Korea (NRF) grant funded by the Korea government (No. 2012-006087). Funding for the SDSS and SDSS-II has been provided by the Alfred P. Sloan Foundation, the Participating Institutions, the National Science Foundation, the U.S. Department of Energy, the National Aeronautics and Space Administration, the Japanese Monbukagakusho, the Max Planck Society, and the Higher Education Funding Council for England. The SDSS Web Site is <http://www.sdss.org/>.

REFERENCES

- Abazajian, K. N., et al. 2009, *ApJS*, 182, 543
 Alatalo, K., et al. 2011, *ApJ*, 735, 88
 Antonucci, R. R. J. & Miller, J. S. 1985, *ApJ*, 297, 621
 Bae, H.-J., Woo, J.-H., Yagi, M., Yoon, S.-J., & Yoshida, M. 2012, *ApJ*, 753, 10
 Baldwin, J. A., Phillips, M. M., & Terlevich, R. 1981, *PASP*, 93, 5
 Barbosa, F. K. B., Storchi-Bergmann, T., Cid Fernandes, R., Winge, C., & Schmitt, H. 2009, *MNRAS*, 396, 2
 Blecha, L., Loeb, A., & Narayan, R. 2013, *MNRAS*, 429, 2594
 Boroson, T. 2005, *AJ*, 130, 381
 Calzetti, D. 1999, *ApSS*, 266, 243
 Campanelli, M., Lousto, C., Zlochower, Y., & Merritt, D. 2007, *ApJ*, 659, L5
 Cappellari, M., & Emsellem, E. 2004, *PASP*, 116, 138
 Cecil, G., Bland-Hawthorn, J., Veilleux, S., & Filippenko, A. V. 2001, *ApJ*, 555, 338
 Choi, Y.-Y., Han, D.-H., & Kim, S. S. 2010, *JKAS*, 43, 191
 Ciotti, L., Ostriker, J. P., & Proga, D. 2009, *ApJ*, 699, 89
 Comerford, J. M., et al. 2009, *ApJ*, 698, 956
 Comerford, J. M., & Greene, J. E. 2014, *ApJ*, 789, 112
 Crenshaw, D. M., Kraemer, S. B. 2000, *ApJ*, 532, L101
 Crenshaw, D. M., Kraemer, S. B., Hutchings, J. B., et al. 2000, *AJ*, 120, 1731
 Crenshaw, D. M., Kraemer, S. B., & George, I. M. 2003, *ARA&A*, 41, 117
 Crenshaw, D. M., Schmitt, H. R., Kraemer, S. B., Mushotzky, R. F., & Dunn, J. P. 2010, *ApJ*, 708, 419
 Croton, D. J., et al. 2006, *MNRAS*, 365, 11
 Das, V., et al. 2005, *AJ*, 130, 945
 De Young, D. S. 2010, *ApJ*, 710, 743
 Dubois, Y., Gavazzi, R., Reirani, S., & Silk, J. 2013, *MNRAS*, 433, 3297
 Ferrarese, L., & Merritt, D. 2000, *ApJ*, 539, L9
 Fischer, T. C., Crenshaw, D. M., Kraemer, S. B., Schmitt, H. R., & Tripp, M. L. 2010, *AJ*, 140, 577
 Fischer, T. C., Crenshaw, D. M., Kraemer, S. B., & Schmitt, H. R. 2013, *ApJS*, 209, 1
 Gebhardt, K., et al. 2000, *ApJ*, 539, L13
 Greene, J. E., Zakamska, N. L., & Smith, P. S. 2012, *ApJ*, 746, 86
 Gültekin, K., et al. 2009, *ApJ*, 698, 198
 Heckman, T. M. 1980, *A&A*, 87, 152
 Heckman, T. M. 2004, *ApJ*, 613, 109
 Kauffmann, G., et al. 2003, *MNRAS*, 346, 1055

- Kewley, L. J., Dopita, M. A., Sutherland, R. S., Heisler, C. A., & Trevena, J. 2001, *ApJ*, 556, 121
- Kewley, L. J., Groves, B., Kauffmann, G., & Heckman, T. 2006, *MNRAS*, 372, 961
- Kimball, A. E., & Ivezić, Ž 2008, *AJ*, 136, 684
- Komossa, S., & Xu, D. 2007, *ApJ*, 667, L33
- Komossa, S., Xu, D., Zhou, H., Storchi-Bergmann, T., & Binette, L. 2008, *ApJ*, 680, 926
- Kormendy, J., & Ho, L. C. 2013, *ARA&A*, 51, 511
- LaMassa, S. M., et al. 2009, *ApJ*, 705, 568
- Lintott, C. et al. 2011, *MNRAS*, 410, 166
- Markwardt, C. B. 2009, *ASPC*, 411, 251
- McConnell, N. J., & Ma, C.-P. 2013, *ApJ*, 764, 184
- Merrit, D., et al. 2006, *MNRAS*, 367, 1746
- Milosavljević, M., & Merritt, D. 2001, *ApJ*, 563, 34
- Müller-Sánchez, F. et al. 2011, *ApJ*, 739, 69
- Nath, B. B., & Silk, J. 2009, *MNRAS*, 396, L90
- Nelson, C. H., & Whittle, M. 1995, *ApJS*, 99, 67
- Netzer, H. 2009, *MNRAS*, 399, 1907
- Park, D., Kelly, B. C., Woo, J.-H., & Treu, T. 2012, *ApJS*, 203, 6
- Puchwein, E. & Springel, V. 2013, *MNRAS*, 428, 2966
- Ruiz, J., et al. 2001, *AJ*, 122, 2961
- Ruiz, J. R., Crenshaw, D. M., Kraemer, S. B., et al. 2005, *AJ*, 129, 73
- Sánchez-Blázquez, P., et al. 2006, *MNRAS*, 371, 703
- Sarzi, M., et al. 2006, *MNRAS*, 366, 1151
- Shankar, F., Weinberg, D. H., & Miralda-Escudé, J. 2013, *MNRAS*, 428, 421
- Shen, Y., Liu, X., Greene, J. E., & Strauss, M. A. 2011, *ApJ*, 735, 48
- Sugai, H. et al. 2005, *ApJ*, 629, 131
- Veilleux, S., Cecil, G., & Balnd-Hawthorn, J. 2005, *ARA&A*, 43, 769
- Veilleux S., & Osterbrock D. E., 1987, *ApJS*, 63, 295
- Wang, J., Mao, Y. F., & Wei, J. Y. 2011, *ApJ*, 741, 50
- White, R. L., Becker, R. H., Helfand, D. J., & Gregg, M. D. 1997, *ApJ*, 475, 479
- Woo, J.-H., Kim, J. H., Imanishi, M., & Park, D. 2012, *AJ*, 143, 49
- Woo, J.-H., et al. 2013, *ApJ*, 772, 49
- Zamanov, R., et al. 2002, *ApJ*, 576, L9
- Zhang, K., Dong, X.-B., Wang, T.-G., & Gaskell, C. M. 2011, 737, 71